Article

Transient Disruption of the Inferior Parietal Lobule Impairs the Ability to Attribute Intention to Action

Highlights

- Perturbation of inferior parietal lobule (IPL) impairs intention to action mapping

- Inferior frontal gyrus perturbation does not affect intention reading

- Observers can still discriminate changes in kinematics after IPL perturbation

- IPL perturbation selectively misaligns intention readout to intention encoding

Authors

Jean-François Patri, Andrea Cavallo, Kiri Pullar, ..., Alessio Avenanti, Stefano Panzeri, Cristina Becchio

Correspondence

stefano.panzeri@iit.it (S.P.), cristina.becchio@iit.it (C.B.)

In Brief

Patri et al. combine continuous theta burst stimulation (cTBS) with computational modeling to causally probe single-trial intention computations in fronto-parietal regions. They find that stimulation over the inferior parietal lobule deteriorates mapping from informative kinematic features to intention choices during action observation.

CellPress

Article

Transient Disruption of the Inferior Parietal Lobule Impairs the Ability to Attribute Intention to Action

Jean-François Patri,[1,2] Andrea Cavallo,[1,3] Kiri Pullar,[1,2] Marco Soriano,[1,3] Martina Valente,[2,4] Atesh Koul,[1]
Alessio Avenanti,[5,6] Stefano Panzeri,[2,7,8,*] and Cristina Becchio[1,7,*]

[1]Cognition, Motion & Neuroscience, Center for Human Technologies, Istituto Italiano di Tecnologia, Genoa, Italy
[2]Neural Computation Lab, Center for Human Technologies, Istituto Italiano di Tecnologia, Genoa, Italy
[3]Department of Psychology, University of Turin, Turin, Italy
[4]Center for Mind/Brain Sciences (CIMeC), University of Trento, Rovereto, Italy
[5]Center for Studies and Research in Cognitive Neuroscience, Department of Psychology, University of Bologna, Cesena, Italy
[6]Centro de Investigación en Neuropsicología y Neurociencias Cognitivas, Universidad Católica del Maule, Talca, Chile
[7]Senior author
[8]Lead Contact
*Correspondence: stefano.panzeri@iit.it (S.P.), cristina.becchio@iit.it (C.B.)
https://doi.org/10.1016/j.cub.2020.08.104

SUMMARY

Although it is well established that fronto-parietal regions are active during action observation, whether they play a causal role in the ability to infer others' intentions from visual kinematics remains undetermined. In the experiments reported here, we combined offline continuous theta burst stimulation (cTBS) with computational modeling to reveal and causally probe single-trial computations in the inferior parietal lobule (IPL) and inferior frontal gyrus (IFG). Participants received cTBS over the left anterior IPL and the left IFG *pars orbitalis* in separate sessions before completing an intention discrimination task (discriminate intention of observed reach-to-grasp acts) or a kinematic discrimination task unrelated to intention (discriminate peak wrist height of the same acts). We targeted intention-sensitive regions whose fMRI activity, recorded when observing the same reach-to-grasp acts, could accurately discriminate intention. We found that transient disruption of activity of the left IPL, but not the IFG, impaired the observer's ability to attribute intention to action. Kinematic discrimination unrelated to intention, in contrast, was largely unaffected. Computational analyses of how encoding (mapping of intention to movement kinematics) and readout (mapping of kinematics to intention choices) intersect at the single-trial level revealed that IPL cTBS did not diminish the overall sensitivity of intention readout to movement kinematics. Rather, it selectively misaligned intention readout with respect to encoding, deteriorating mapping from informative kinematic features to intention choices. These results provide causal evidence of how the left anterior IPL computes mapping from kinematics to intentions.

INTRODUCTION

When watching others in action, we readily infer their intentions from subtle changes in the way they move. Theoretical work [1–6] and related experimental findings (e.g., [7–11]) suggest that the ability to read the intention of an observed action is mediated by the fronto-parietal action observation network. However, the specific neural computations involved in this ability remain unclear [12].

A major difficulty in studying how intentions are inferred from others' actions is the ever-changing nature of movement kinematics [13, 14]. Movement is "repetition without repetition" [15]. Averaging across repeats of nominally identical but actually different motor acts, as done in trial-averaged analyses, can obscure how intention information is encoded in trial-to-trial variations in movement kinematics [16]. More importantly, the brain does not operate according to an average response over averaged kinematics. Real-world intention attribution requires a

real-time estimate of intention information encoded within an observed motor act, which can only be captured using readouts of single-trial kinematics.

Here we developed a novel analysis framework for understanding how intention readout maps to the multiplicity of kinematic patterns with single-trial resolution. This framework was inspired by recent mathematical advances in determining how sensory information encoded in a neural population is read out to inform single-trial behavioral choice [17–19]. In this study, we adapted this approach to causally probe single-trial intention readout computations in two core regions of the action observation network: the left inferior parietal lobule (IPL) and the left inferior frontal gyrus (IFG) [10, 11, 20–28].

In both regions, neural responses to observed actions are modulated by intention, operationally defined as the overall goal of a two-step action sequence [2]. In monkeys, IPL (area PFG) and IFG (area F5) neurons responsive during observation of
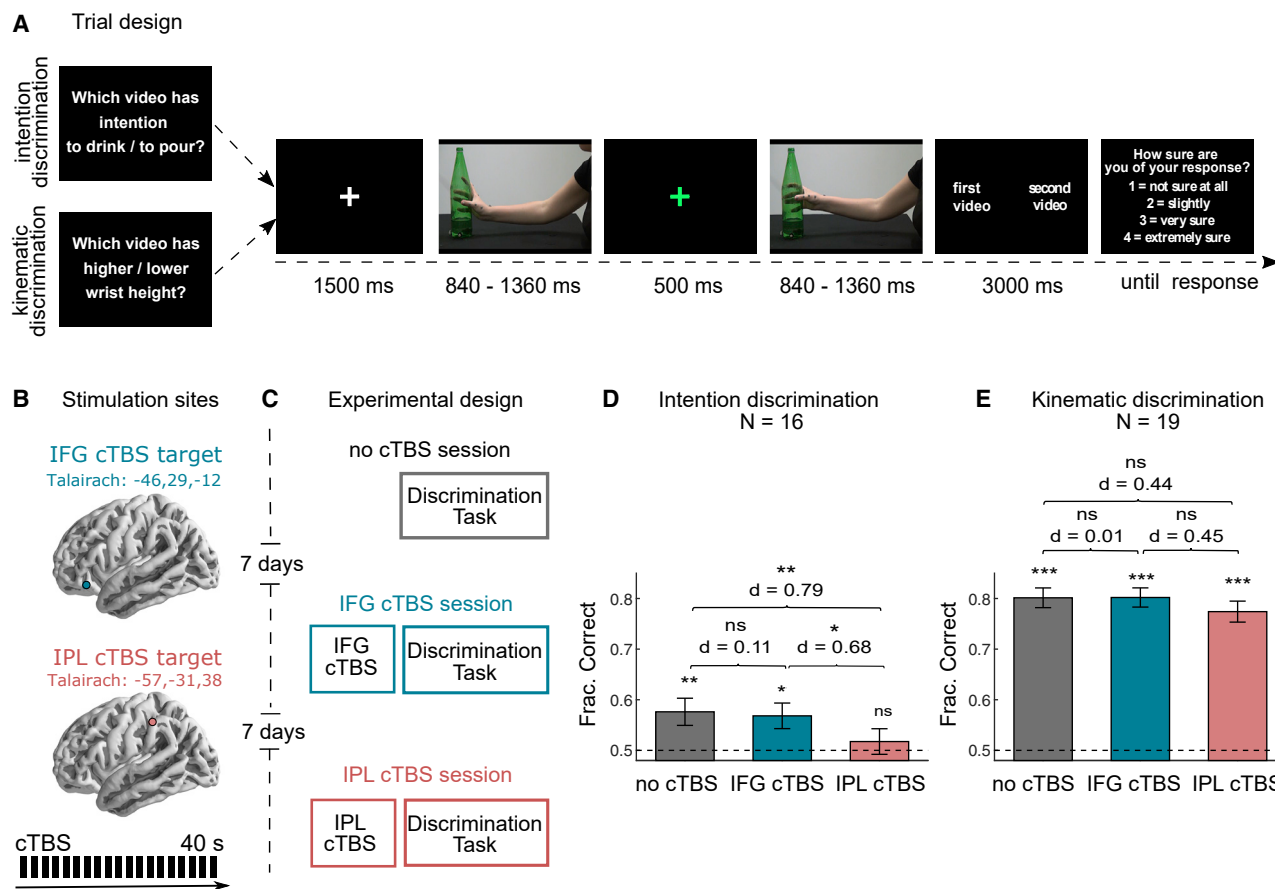
A   Trial design

B Stimulation sites   **C** Experimental design   **D** Intention discrimination N = 16   **E** Kinematic discrimination N = 19

Figure 1. Experimental Design and Behavioral Discrimination Results

(A) Trial design of the discrimination tasks.

(B) cTBS targets and MRI-guided cTBS protocol.

(C) Sketch of the experimental design.

(D and E) Discrimination performance (fraction correct) in the intention discrimination task and the kinematic discrimination task. Histograms represent mean ± SEM across participants. The number of participants in each task (N) and Cohen's effect size (d) of each comparison are reported. * indicates p < 0.05, ** indicates p < 0.01, *** indicates p < 0.001, and ns indicates p > 0.05.

See also Figure S1.

grasping actions are tuned to the intention of the observed act (for example, they respond more vigorously when the observed grasp is performed with the intent to eat rather than to place) [7, 8]. In humans, a distributed pattern of activity within the IPL and IFG can discriminate the intention of observed grasp-to-pour and grasp-to-drink acts [29]. These results suggest that the IPL and IFG contain information about the intention of an observed action. However, the relationship between such information and intention attribution remains correlational [30, 31]. Moreover, simple observation of neural activity cannot determine which features of neural representations are read out and which neural computations affect downstream processing [17, 32, 33]. The contribution of the IPL and IFG to intention attribution, in terms of function (do the IPL and IFG play a causal role in attribution of intention to action?) and content (what and how do the IPL and IFG compute?) remains largely undefined [12].

To investigate these questions, we applied continuous theta burst transcranial magnetic stimulation (cTBS) to reversibly reduce cortical excitability in the left anterior IPL and the left IFG

pars orbitalis at two intention-sensitive locations determined based on re-analysis of fMRI data collected during observation of the same action stimuli as used in the present study [29]. We investigated how transient disruption of activity in these regions influences readout computations involved in extracting intention-related information from observed grasping acts. Single-trial analyses combined with a set of task manipulations revealed that disruption of activity in the left anterior IPL, but not the left IFG *pars orbitalis*, impaired an observer's ability to interpret the intentional significance of changes in discriminative kinematic features.

RESULTS

Causal Contribution of the IPL to Intention Discrimination

To perturb fronto-parietal sites within the action observation network, we used a cTBS protocol delivered offline for 40 s [26, 34, 35]. In three separate sessions, participants (n = 16) received no cTBS or magnetic resonance imaging (MRI)-guided cTBS to

the left IPL or left IFG before completing a two-alternative, forced-choice (2AFC) discrimination of intention (Figures 1A–1C).

To capture natural movement variability, we selected 60 representative reach-to-grasp acts, 30 for each intention, from a large dataset obtained by filming naive participants reaching toward and grasping a bottle with the intent to drink or pour. Each trial displayed two reach-to-grasp acts in two consecutive temporal intervals: one interval contained a grasp-to-pour act and the other interval a grasp-to-drink act. Participants were required to indicate, in each trial, the interval displaying the reach-to-grasp act performed with the intent to drink (or to pour; STAR Methods), and, at the end of the trial, to rate the confidence of their choice (Figure 1A).

Individual targets for cTBS were determined based on re-analysis of fMRI data [29] recorded during the observation of the same action stimuli as used in this study. We defined separate anatomical regions of interest (ROIs) for the left and the right IFG *pars opercularis*, *pars triangularis*, and *pars orbitalis* and for the left and right IPL. We ran separate cross-validated linear support vector machine (SVM) classifiers within each ROI. cTBS was applied to the ROIs with the highest decoding accuracies (left IFG *pars orbitalis* and left IPL). Target regions in the *pars orbitalis* of the left IFG and in the anterior portion of the left IPL were identified as locations containing a high proportion of discriminative (top 20%) voxels (Figure S1A; Table S1).

We used logistic mixed effects models (LMEMs) [36] to test statistically whether average intention discrimination performance differed from chance and across sessions. Discrimination performance, computed as the fraction of correct responses, was above chance in no cTBS and IFG cTBS but not in IPL cTBS (Figure 1D; Table S3). A likelihood ratio test from LMEMs revealed a main effect of cTBS on discrimination performance (Table S3), driven by a decrease in intention discrimination after IPL cTBS relative to no cTBS and IFG cTBS (Figure 1D). The effect of IFG cTBS relative to no cTBS was not significant (Figure 1D). We also found no significant differences across sessions in confidence ratings (Table S3). This suggests that cTBS to the IPL, but not to the IFG, impaired the ability to discriminate intention.

Discrimination of Individual Kinematic Features following cTBS

To investigate the selectivity of the effects reported above to intention discrimination, we tested a new cohort of participants (n = 19) carrying out a 2AFC kinematic discrimination task unrelated to intention. Action stimuli and task parameters were identical to that of the intention discrimination task except that participants were required to discriminate differences in the peak wrist height of the observed acts. We found no main effect of cTBS on kinematic discrimination (Table S3). As shown in Figure 1E, the effect of cTBS to the IPL (or IFG) on kinematic discrimination performance was smaller and not significant. This suggests that, following IPL and IFG cTBS, observers retained the ability to detect changes in individual kinematic features when instructed to do so.

We were concerned that lack of cTBS effects on kinematic discrimination might be related to the relative ease of the kinematic task. To control for task difficulty, we ranked trials in each task based on intention-related information encoded in movement kinematics (Figure S1C) and restricted the analyses to the 10% most informative trials for intention discrimination

and the 10% least informative trials for kinematic discrimination. With this selection of trials, kinematic discrimination performance did not differ from intention discrimination performance under no cTBS. Nonetheless, and consistent with results utilizing all trials, the effect of IPL cTBS relative to no cTBS and IFG cTBS on intention discrimination persisted with large effect size. In contrast, cTBS (to the IPL or IFG) had no significant effect on kinematic discrimination even with performance-matched trial subsampling (Figure S1C). Collectively, these analyses suggest that IPL cTBS did not impair the ability to discriminate changes in individual kinematic features.

Using Logistic Regression to Relate Intention Encoding and Readout at the Single-Trial Level

Having demonstrated that IPL cTBS selectively impairs trial-averaged intention discrimination, we next developed a new analysis framework to dissect single-trial computations involved in reading out intention information encoded in movement kinematics. Intention encoding (mapping of intention to movement kinematics) and intention readout (mapping of kinematics to intention choice) are commonly studied as separate processes [3]. One limitation of this approach is that it cannot determine the contribution of specific kinematic features to task performance [17, 37]. For example, separate encoding and readout analyses may show that two kinematic features carry intention (encoding) information and intention choice (readout) information. However, one feature is read out correctly and aids intention discrimination, whereas the other feature is read out incorrectly and hinders intention discrimination. Here we obviated this limitation by investigating the intersection between intention encoding and intention readout at the single-trial level. We first developed an encoding model to quantify intention information encoded in single movement kinematics and identify intention information-carrying features. We then modeled intention readout to understand how intention information carried by specific kinematic features is read out by human observers in each trial. We finally computed how encoding and readout intersect in each trial to inform intention choice. This approach allowed us to rigorously test a range of hypotheses about how IPL computations contribute to inform intention choice.

Encoding of Intention-Related Information

We represented single-trial kinematics as a vector in the 64-dimensional space of kinematic features spanning 16 kinematic variables over 4 time epochs (see STAR Methods, Figures 2A and 2B, and Table 1 for example of single-trial traces of two kinematic variables). The encoding model used logistic regression to compute the probability of the first interval of each trial to display a grasp-to-drink act (and, thus, of the second interval to display a grasp-to-pour act) as a combination of the features of the kinematic vector for that trial [38] (Figures 2C and 2D).

Figure 2E shows a geometric sketch of the encoding model in a hypothetical, simplified kinematic space spanning only two kinematic features. The encoding boundary defines the border that best separates the kinematic patterns of the two intentions. The encoding vector, which is orthogonal to the encoding boundary and whose components equal the logistic regression coefficients, indicates the information axis along which changes in kinematics maximally discriminate between intentions. In the kinematic
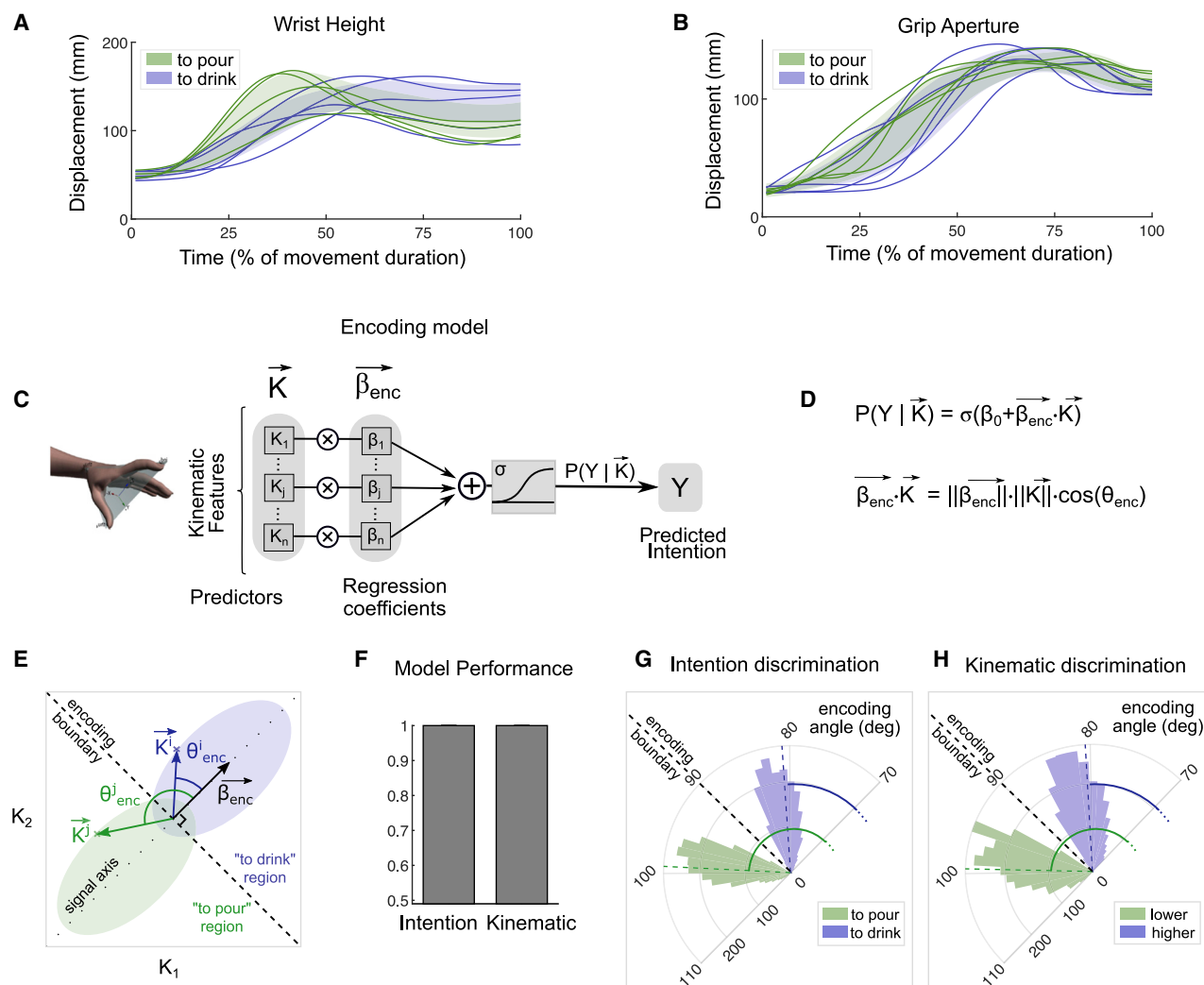
Figure 2. Encoding of Task-Discriminative Information in Movement Kinematics

(A and B) Time course of W_H and grip aperture for reach-to-grasp acts performed with the intent to drink or to pour. Colored curves display representative trajectories for each intention, and colored areas display one standard deviation across executed trials.

(C and D) Schematic of the encoding model. Shown are a block diagram representation and equation of the logistic regression used to quantify intention information in movement kinematics.

(E) Sketch of the encoding model in a simplified kinematic space spanning only two kinematic features (K_1 and K_2). The two elliptical regions represent the intention conditional probability distributions of the two features. The encoding boundary optimally separates the kinematics patterns into "to drink" and "to pour" regions. The encoding vector $\overrightarrow{\beta_{enc}}$ indicates the maximally discriminative axis. The angle θ_{enc} between the encoding vector and the single-trial kinematic vector $\overrightarrow{K}$ can be used to classify single trials according to intention. Two different single-trial kinematic vectors with superscript i and j are shown.

(F) Performance of the encoding models, quantified as the fraction of correctly predicted trials (mean ± SEM across participants).

(G and H) Polar plot of the distribution of encoding angles across trials in the intention discrimination task and the kinematic discrimination task. For graphical representation, the angle range is expanded so that angles of 70°–110° are mapped to a semicircle.

See also Figure S2.

feature space, single-trial kinematic vectors are classified as "to pour" or "to drink," depending on which side of the boundary they fall or, equivalently, according to the angle they form with the encoding vector. Because in our convention the encoding vector points toward "to drink," 0°–90° encoding angles indicate "to drink," whereas 90°–180° encoding angles indicate "to pour."

As shown in Figure 2G, "to pour" and "to drink" angle distributions were perfectly separable, being narrowly distributed approximately 8° either side of the intention-encoding boundary

(90°)—a set of angles corresponding to the diagonals in the 64-dimensional kinematic feature space (Figures S2E–S2G). Importantly, with all single-trial kinematic vectors pointing toward the correct intention (Figure 2G), intention encoding reached perfect accuracy (Figure 2F). This indicates that, despite the variability of kinematic features across trials, variation in grasping kinematics fully specified intention information in each trial. As expected by task design, single-trial variations also fully specified peak wrist height information (Figures 2F and 2H).
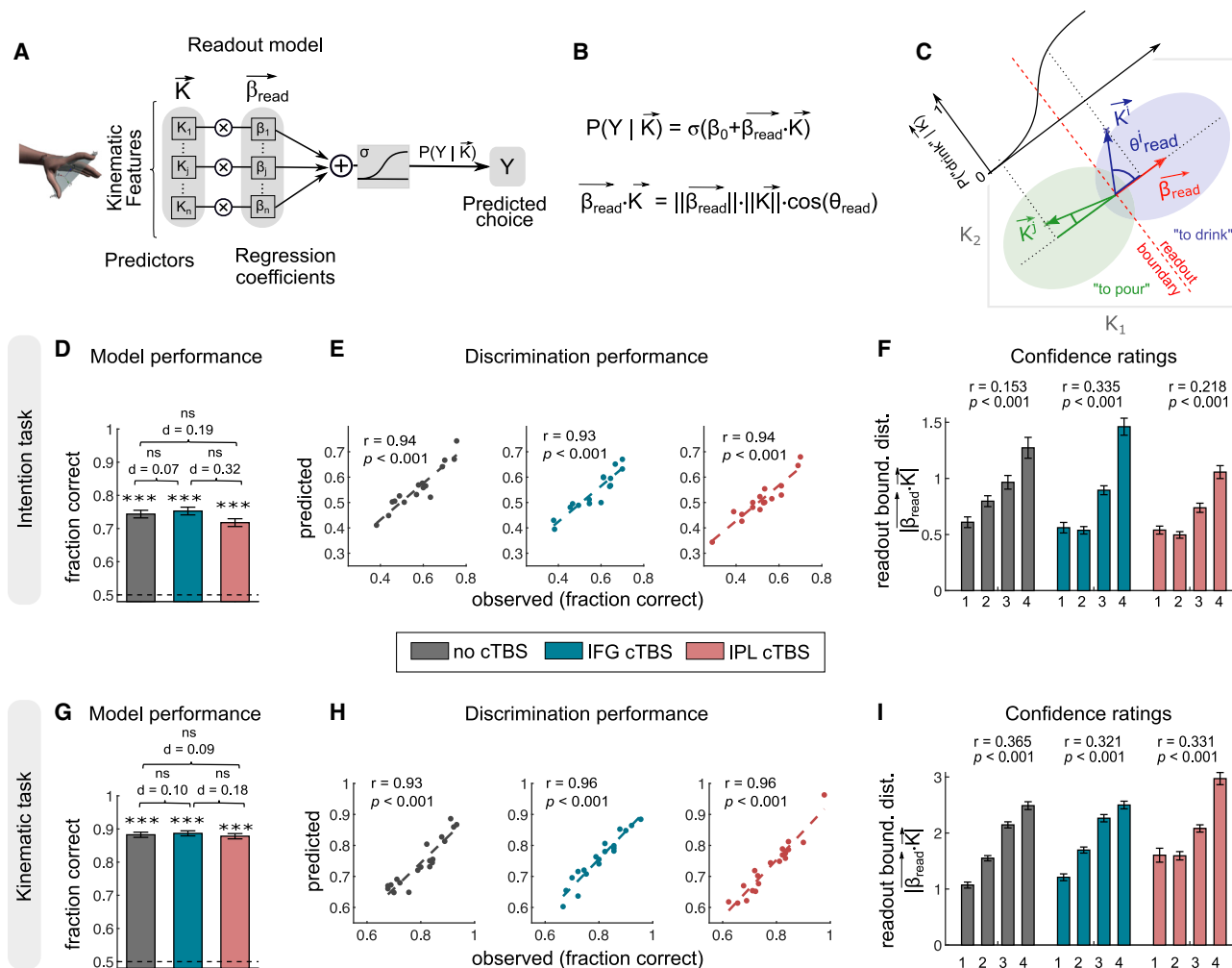
Figure 3. Readout Model of Intention Discrimination from Single-Trial Kinematics

(A and B) Readout model. Shown are a block diagram representation and equation of the logistic regression used to quantify intention information readout.

(C) Sketch of the readout model in a simplified kinematic space spanning only two kinematic features. The two elliptical regions represent the probability distributions of the two features conditional to intention choice. The readout vector $\overrightarrow{\beta_{read}}$ of regression coefficients indicates the direction in feature space that maximally discriminates observers' choices. The direction and distance of the single-trial kinematic vector from the readout boundary determine, through the sigmoid logistical function, the probability of intention choice in that trial.

(D) Performance of the readout model in predicting observers' choices in the intention discrimination task, quantified as fraction of correctly predicted trials.

(E) Scatterplots of the relationship between the observed discrimination performance and the one predicted by the readout model across individual participants in the intention discrimination task.

(F) Distance of the single-trial kinematic vector from the readout boundary as a function of confidence ratings for the intention discrimination task. This distance was computed as the modulus of the scalar product between the single-trial kinematic vector and the readout vector. As shown in (C), the larger this distance, the further from chance is the probability of intention choice predicted by the model. The green single-trial kinematic vector in (C), for example, has a larger distance and, thus, a further-from-chance probability of intention choice than the blue kinematic vector.

(G–I) Same as (D)–(F) for the kinematic discrimination task.

In (D) and (G), Cohen's effect size (d) of each comparison is reported. * indicates $p < 0.05$, ** indicates $p < 0.01$, *** indicates $p < 0.001$, and ns indicates $p > 0.05$. See also Figure S3.

Combined with the above findings of a higher-than-chance but far from perfect trial-averaged performance under no cTBS (about 57% in the intention discrimination task and 82% in the kinematic discrimination task), these results suggest a partial discrepancy between information encoded in grasping kinematics and information readout. Thus, the next question was how human observers read out information encoded in single-trial kinematics.

Readout of Intention-Related Information

We developed a readout model that used logistic regression to predict the probability of intention attribution in each trial as a combination of the features of the kinematic vector for that trial (Figures 3A–3C). Figure 3C sketches the readout model in a hypothetical 2-dimensional kinematic space. Similar to what is described above for the encoding model, the readout boundary defines the border in kinematic space best separating the two

choices. The readout vector, orthogonal to the readout boundary and with components equal to the logistic regression coefficients, indicates the axis with maximal choice information.

We fitted the readout model, separately for each participant, to single-trial intention choices and used confidence ratings reported by observers for independent validation of the model. Readout models were estimated separately for each participant for no cTBS, IPL cTBS, and IFG cTBS sessions. Across trials and participants, model performance, measured as the fraction of intention choices correctly predicted by the model, was significantly above chance (Figure 3D).

Although confidence ratings were not used for fitting model parameters, we also found a positive trial-to-trial relationship between the observer's confidence in his or her intention choice and the distance of the single-trial kinematics vector from the readout boundary—the border that best separates kinematic patterns for the two intention choices (Figure 3F). This suggests that intention choices in trials farther away from the readout boundary (and thus classified with greater confidence by the model) were also endorsed with higher confidence by human observers. Similar results were obtained for a readout model using single-trial differences in movement kinematics to predict kinematic discrimination (Figures 3G–3I).

Collectively, the above analyses suggest that our readout model was able to capture task performance, providing a plausible description of how well and how confidently observers performed the discrimination tasks based on single-trial kinematics.

Transient Disruption of the IPL Does Not Decrease Sensitivity of Intention Readout to Movement Kinematics

Having verified that our readout model could account for discrimination performance, we next used it to test alternative hypotheses regarding the cause of the decrease in intention discrimination following IPL cTBS (Figure 1C). First, we considered the possibility that cTBS over the IPL decreases the sensitivity of intention readout to single-trial variations in movement kinematics. This hypothesis predicts that the statistical dependency between single-trial kinematics and intention choice is weaker following IPL cTBS. To test this formally, we compared the fraction of intention choices correctly predicted by the model across sessions. We found no difference between no cTBS, IPL cTBS, and IFG cTBS (Figure 3D), suggesting that diminished sensitivity of intention readout to kinematics cannot account for the inferior discrimination performance following IPL cTBS. Corroborating this proposition, the average norm of the readout vector, which is a measure of the strength of the readout [39], did not vary across sessions (Table S4). Finally, the number of non-zero readout coefficients also did not vary across sessions (Table S4), suggesting that IPL cTBS did not impair the ability to gather information from different kinematic features.

Transient Disruption of the IPL Causes Misalignment of Intention Readout with Respect to Encoding

Having established that IPL cTBS does not influence the overall sensitivity of intention readout to kinematics, we next considered the hypothesis that IPL cTBS alters the ability to correctly read out intention-related information encoded in movement

kinematics. An intuitive visualization of how well readout captures intention-related information in movement kinematics is provided by the angle between the encoding vector and the readout vector orthogonal to the readout boundary (Figures 4A and 4B). The smaller the angle between these vectors, the larger the across-trial alignment between intention encoding and readout in kinematic space and, thus, the larger the probability that intention information is read out correctly across trials.

At the single-trial level, alignment can be computed as the angle between the single-trial kinematic vector and the readout vector. Angles of 90° indicate that readout is unrelated to encoded intention information, angles lower than 90° (Figure 4A) indicate correct (incorrect) readout of intention information for "to drink" ("to pour") trials, and angles higher than 90° (Figure 4B) indicate correct (incorrect) readout of intention information for "to pour" ("to drink") trials.
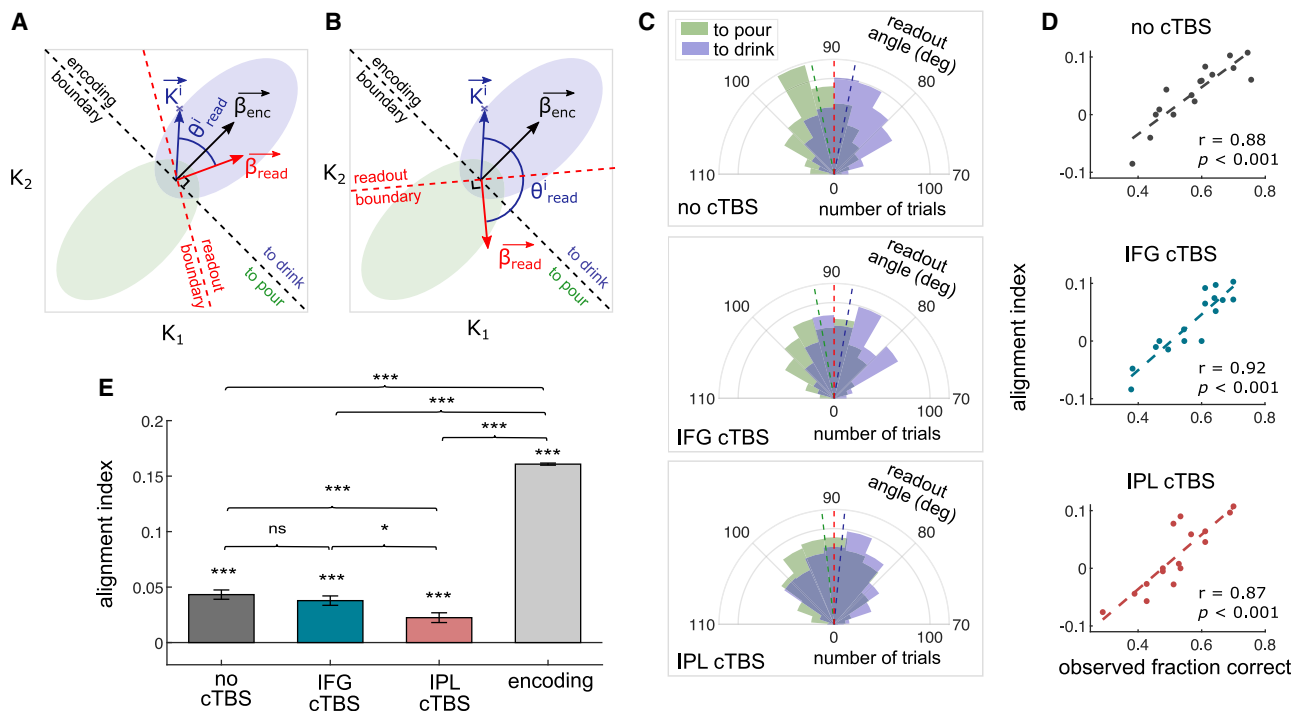
As shown in Figure 4C, under no cTBS (and IFG cTBS), single-trial angle distributions were centered 3° away from the readout boundary (90°) and 5° off the diagonal in the 64-dimensional kinematic feature space (along which the encoding angles are distributed). Critically, "to pour" and "to drink" distributions only partly overlapped, with the majority of trials (64%) distributed in the correct readout angle range.

For IPL cTBS, single-trial angles were centered only 1° away from the readout boundary, with an almost complete overlap between intention-specific distributions and with about half of the trials in the incorrect readout angle range (Figure 4C). These data suggest that IPL cTBS impaired the ability to correctly read out intention information encoded in single-trial kinematics.

To quantify these observations, we devised a single-trial alignment index based on the projection of the single-trial kinematic vector on the readout vector. Although the projection is a signed value, we adjusted the sign so that positive (negative) alignment indices denoted correct (incorrect) readout (STAR Methods). Consistent with the intuition conveyed in Figure 4C, the results revealed a significant decrease in alignment after IPL cTBS in comparison with no cTBS and IFG cTBS (Figure 4E). To rule out that such a decrease could be accounted for by small (and not significant) differences in model performance across sessions, we repeated the analyses, considering only trials correctly predicted by the model. The pattern of results remained highly similar (Figure S4C). For the kinematic discrimination task, no cTBS and IPL cTBS did not differ in alignment (Figures S4A, S4B, S4D, and S4E).

Alignment Predicts Individual Task Performance

To substantiate the link between alignment and individual task performance, we quantified the fraction of behaviorally correct trials at the single-subject level as a function of alignment. For all sessions and tasks, alignment was positively correlated with individual task performance (Figure 4D). Moreover, for the intention and kinematic tasks, the decrease in alignment correlated with the decrease in discrimination performance following IPL cTBS on a subject-by-subject basis (Table S5). Also, alignment was more predictive of individual discrimination performance than other model parameters, such as the norm and number of non-zero readout coefficients (Figure S4). Consistent with the view that alignment reflects correctness rather than confidence of the information readout, the

Figure 4. Misalignment of Readout following IPL cTBS

(A and B) Diagrams illustrating alignment (A) and misalignment (B) between intention encoding and readout in a simplified two-kinematic feature space. Conventions are as in Figures 2E and 3C. The larger the angle between the encoding vector and the readout vector, the larger, on average, the angle between the single-trial kinematic vector and the readout vector. This justifies an alignment index based on the cosine of the angle between the single-trial kinematic vector and the readout vector, with positive alignment indices denoting correct readout.

(C) Polar plot of the distribution of readout angles for "to pour" and "to drink" trials under no cTBS, IFG cTBS, and IPL cTBS. For graphical representation, the 70°–110° angle range is expanded to a semicircle. The dashed red line marks the readout boundary (90°).

(D) Scatterplots of alignment indices against observed task performance across participants under no cTBS, IFG cTBS, and IPL cTBS.

(E) Effect of cTBS on the alignment index. For comparison, we also show the value of the alignment index computed as the signed cosine of the encoding angle θ_{enc}. This angle is close the diagonal line of our 64-dimensional kinematic feature space. As shown in Figure 2G, the angle θ_{enc} between the encoding vector and the single-trial kinematic vector $\vec{K}$ can be used to classify the intention of single-trial kinematics with 100% accuracy. Histograms represent mean ± SEM across all trials and participants. * indicates p < 0.05, ** indicates p < 0.01, *** indicates p < 0.001, and ns indicates p > 0.05. See also Figure S4.

correlation between alignment and confidence ratings was much weaker (Table S5). Together, these results suggest that transient disruption of the IPL selectively misaligned intention readout with respect to encoding.

Origins of Misalignment between Intention Encoding and Readout

To understand the origins of the misalignment induced by IPL cTBS, we further examined the distribution and concordance in sign of readout coefficients relative to encoding coefficients. Given the lack of effect of IFG cTBS at the subject level and trial level, in this analysis we focused on comparing no cTBS and IPL cTBS.

Under no cTBS (and IPL cTBS), observers read out more intention-informative features than expected under the null hypothesis that the non-zero readout weights are assigned randomly to features regardless of their intention information (Table S4). A first possibility is that misalignment results from a shift in the distribution of readout coefficients toward non-informative kinematic features; that is, a larger fraction of non-zero readout coefficients is assigned to non-informative individual kinematic

features after IPL cTBS. Against this hypothesis, we found no difference in the average fraction of non-zero readout coefficients assigned to informative kinematic features between no cTBS and IPL cTBS (Figure 5A; see also Figure S5A for the kinematic discrimination task). A second possible origin of misalignment is that IPL cTBS deteriorates the mapping from informative kinematic features to intention choices. For example, a variation in a particular feature encoding "to drink" (e.g., higher wrist height at 75% of movement duration; Figure 2A), correctly read as "to drink" under no cTBS, might be incorrectly read as "to pour" under IPL cTBS. Geometrically, this would correspond to the readout vector and the encoding vector pointing in opposite directions (Figure 4B); that is, the coefficients of the readout vector and of the encoding vector for the considered feature having opposite signs. Consistent with this hypothesis, the fraction of non-zero readout coefficients correctly aligned to informative kinematic features was lower in IPL cTBS compared with no cTBS in the intention discrimination task (Figure 5B) but not in the kinematic discrimination task (Figure S5B). Together, these analyses indicate that cTBS to the left IPL altered mapping of informative kinematic features to intention choices.
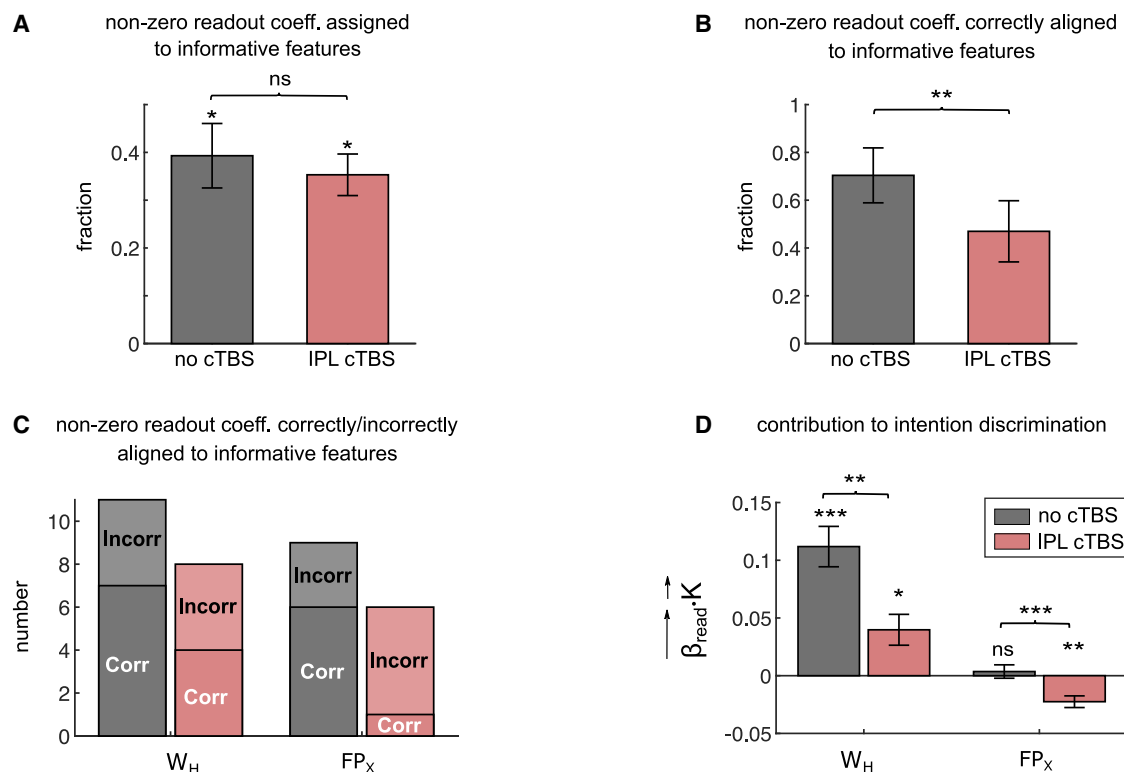
Figure 5. Origins of Misalignment

(A) Fraction of non-zero readout coefficients assigned to informative features.

(B) Fraction of non-zero readout coefficients assigned to informative features and correctly aligned with encoding. Fraction was computed on a subject basis and then averaged across subjects.

(C) Number of non-zero readout coefficients (in)correctly aligned to informative features in encoding. We focused on the most informative and most read out kinematic variable: the height of the wrist (W_H) and the relative abduction/adduction of the thumb and the index finger, irrespective of wrist rotation (FP_X).

(D) Contribution of W_H and FP_X to intention discrimination performance, computed as the scalar product between the kinematic vector and the readout vector within that feature subspace.

Histograms represent mean ± SEM across all trials and participants. * indicates $p < 0.05$, ** indicates $p < 0.01$, *** indicates $p < 0.001$, and ns indicates $p > 0.05$. See also Figure S5.

IPL cTBS Alters Readout of the Two Most Informative Kinematic Features

To gain further insight into the inter-individual reproducibility of readout, we explored how specific features were read by different observers by computing cross-correlations between individual-participant readout coefficients. Observers showed low cross-correlation between readout coefficients (mean ± SEM: 0.06 ± 0.02 for no cTBS, 0.03 ± 0.03 for IFG cTBS, 0.02 ± 0.01 for IPL cTBS), attesting to a diverse range of individual readout patterns.

Strikingly, under no cTBS, the two variables that were read out more consistently across observers (Figure S2C) were also more informative over a wider time range in terms of encoding (Figure S2A): the height of the wrist (W_H) and the relative abduction/adduction of the thumb and the index finger (FP_X). Under no cTBS, W_H and FP_X, readout weights correctly aligned with respect to encoding outnumbered incorrectly aligned readout weights (Figure 5C). IPL cTBS decreased the number of correctly aligned readout weights for both kinematic variables. For FP_X, but not for W_H, this decrease was accompanied by an increase in the number of incorrectly aligned readout weights.

To estimate the implications of these readout patterns for single-trial discrimination performance, we computed an index of how much W_H and FP_X contributed to correct intention choice. This index was computed as the scalar product between the kinematic vector and the readout vector within the kinematic subspace formed by each variable. We adjusted the sign so that positive (negative) values of this index indicate a positive (negative) contribution to the correct choice. As shown in Figure 5D, the contribution of both features to single-trial task performance decreased after IPL cTBS. Consistent with the pattern in Figure 5C, for FP_X, but not for W_H, the contribution changed from null to negative, suggesting that, following IPL cTBS, incorrect readout of FP_X contributed to decreased task performance. For the kinematic discrimination task, IPL cTBS had no influence on how the most informative variables, including W_H, were read out (Figures S5C and S5D). These findings fit well with the above reported result of a task-selective decrease in alignment between encoding and readout after IPL cTBS and confirm that, although IPL is not necessary for processing of intention-informative kinematic features, it is necessary for mapping such features to intention choices.

DISCUSSION

The contribution of the IPL and IFG to intention reading has been a matter of long-standing debate [4, 5]. As demonstrated by previous studies and confirmed by our re-analysis of fMRI data [29], these regions contain intention-related information. However, what they compute and whether these computations play a causal role in attribution of intention to action was undetermined. Here, we developed a novel approach, combining offline cTBS with kinematic analysis and computational methods inspired by neural information coding, to causally probe single-trial computations in the left anterior IPL and the left IFG *pars orbitalis*. This approach allowed us to draw inferences about how intention encoding and readout intersect at the single-trial level and the role of the left anterior IPL in mapping kinematics to intention.

Many accounts of intention reading assume kinematics to be equivocally related to intention [5, 6, 40, 41]. Contrary to this assumption, our combined experimental and modeling results indicate that, in our dataset, single-trial variations in movement kinematics fully discriminate between alternative intentions. In the absence of perturbation of neural activity, intention discrimination relies on the readout of encoded information. These findings support the previously proposed idea that human observers use subtle variations in movement kinematics to attribute intention [2, 3]. An important advance of the current study is use of an analysis intersecting encoding and readout at the single-trial level to determine the set of kinematic features carrying intention information that is read out to inform behavioral choice. This analysis proved that the pattern of readout is sparse and idiosyncratic but not random. Under no cTBS, informative features are selected for readout more and read more correctly than expected by chance. Notably, the two features informative over a wider time range in terms of encoding are also the two features more consistently read out across individual observers. Hence, in sessions where no stimulation occurs, observers consistently rely on kinematic features carrying more intention information. This suggest that, although readout only partially exploits the intention information encoded in movement kinematics, it nevertheless prioritizes the most diagnostic features.

Transient disruption of the left anterior IPL did not impair the ability to discriminate changes in specific kinematic features, nor did it alter the relative weight given to informative versus non-informative features. Rather, it selectively decreased alignment between intention encoding and readout, affecting the observer's ability to link variation in informative kinematic features to the correct intention. Together with previous brain stimulation studies targeting left anterior IPL [42] (rather than more posterior and dorsal sectors of the parietal cortex [22, 26]), these results provide causal support for an architecture in which the left anterior IPL represents goals or intentions and is placed at the highest level of the cortical hierarchy engaged during action observation [4]. Kinematics and intention are often conceptualized and examined as relatively independent levels of such a hierarchy [2], leading some authors to interpret the responsivity of IPL neural populations as being tuned to intention as opposed to kinematics [8]. Our finding that transient disruption of activity in the left anterior IPL affects the correct readout of informative kinematic features suggests that the responsivity of IPL neurons to

kinematics should be reconsidered. We propose that, although neurons in the left anterior IPL do not code variations in informative kinematic features, they are necessary for mapping variations to intention.

In the context of hierarchical models of action observation [4], it may be surprising that transient disruption of the left IFG did not affect intention discrimination. Monkey and human studies relate the left IFG to intention coding [7, 9, 29]. Moreover, there is evidence that, in humans, repetitive transcranial magnetic stimulation (TMS) applied to the left IFG *pars opercularis* impairs interpretation of the observed kinematic patterns [27, 43]. The lack of behavioral modulation induced by cTBS to the IFG *pars orbitalis* in our study may indicate that, although potentially accessible to a classifier (remember that, within the IFG, the left IFG *pars orbitalis* showed the highest sensitivity in our re-analysis of fMRI data), intention information in the left IFG *pars orbitalis* does not functionally contribute to intention attribution.

In our design, the context in which the action was observed did not provide intention-discriminative information. It remains to be seen whether cTBS over the IFG *pars orbitalis* impairs estimation of intention from context. This possibility is consistent with a two-pathway model of action understanding postulating a functional dissociation of abstract (contextual) and progressively more concrete (kinematic) representations of observed actions along the rostral-caudal axis of the IFG [5]. Perturbation of different IFG sites (including the IFG *pars opercularis*), with selective manipulation of contextual and kinematic features, would be needed to test this model causally and interpret our non-results regarding the IFG.

The set of analytical methods developed in the current framework could be further generalized to examine hierarchical dependencies between the left anterior IPL and other intention-sensitive regions within the action observation network, such as the superior temporal sulcus, implicated in analysis of visual kinematics [42, 44, 45]. Finally, our approach could be useful for developing intuition about how atypical encoding and readout link to deficits in social cognition [46]. For example, individuals with autism spectrum conditions are reported to have difficulties perceiving, predicting, and interpreting the actions of others [47]. The analysis and methods presented here could be useful tools for generating and testing alternative hypotheses about how altered readout computations affect the ability to make inferences about others' mental states.

STAR★METHODS

Detailed methods are provided in the online version of this paper and include the following:

- KEY RESOURCES TABLE
- RESOURCE AVAILABILITY
  - Lead Contact
  - Materials Availability
  - Data and Code Availability
- EXPERIMENTAL MODEL AND SUBJECT DETAILS
- METHOD DETAILS
  - Experimental design and procedures
- QUANTIFICATION AND STATISTICAL ANALYSIS
  - Data preprocessing

- Single-trial kinematic vector
- Logistic regression models of encoding and readout
- Training logistic regression models
- Verification of the statistical significance of non-zero regression coefficients
- Encoding model
- Readout model
- Evaluation of model performance
- Computation of task performance predicted by the readout model
- Classification of individual kinematic features as informative
- Contribution of individual kinematic variables to discrimination performance
- Computation of cross-correlations of readout coefficients across participants
- Conventions for p values
- Logistic Mixed Effects Models for assessing statistical differences in the distribution of binary variables
- Permutation test for assessing statistical differences in readout coefficients and alignment
- Statistical significance of correlations

AUTHOR CONTRIBUTIONS

C.B. and S.P. conceived and supervised the project. C.B. and A.C. designed the experiments. S.P., C.B., and J.-F.P. designed the analyses. M.S. and A.K. performed the experiments. J.-F.P., K.P., and A.C. performed the analyses with contributions from M.V. A.A. advised on cTBS. C.B., S.P., and J.-F.P. wrote the manuscript with input from K.P., A.C., and A.A. All authors commented on the text.

DECLARATION OF INTERESTS

The authors declare no competing interests.

REFERENCES

1. Baldwin, D.A., and Baird, J.A. (2001). Discerning intentions in dynamic human action. Trends Cogn. Sci. 5, 171–178.

2. Ansuini, C., Cavallo, A., Bertone, C., and Becchio, C. (2015). Intentions in the brain: the unveiling of Mister Hyde. Neuroscientist 21, 126–135.

3. Becchio, C., Koul, A., Ansuini, C., Bertone, C., and Cavallo, A. (2018). Seeing mental states: An experimental strategy for measuring the observability of other minds. Phys. Life Rev. 24, 67–80.

4. Grafton, S.T., and Hamilton, A.F. (2007). Evidence for a distributed hierarchy of action representation in the brain. Hum. Mov. Sci. 26, 590–616.

5. Kilner, J.M. (2011). More than one pathway to action understanding. Trends Cogn. Sci. 15, 352–357.

6. Kilner, J.M., Friston, K.J., and Frith, C.D. (2007). The mirror-neuron system: a Bayesian perspective. Neuroreport 18, 619–623.

7. Bonini, L., Rozzi, S., Serventi, F.U., Simone, L., Ferrari, P.F., and Fogassi, L. (2010). Ventral premotor and inferior parietal cortices make distinct contribution to action organization and intention understanding. Cereb. Cortex 20, 1372–1385.

8. Fogassi, L., Ferrari, P.F., Gesierich, B., Rozzi, S., Chersi, F., and Rizzolatti, G. (2005). Parietal lobe: from action organization to intention understanding. Science 308, 662–667.

9. Iacoboni, M., Molnar-Szakacs, I., Gallese, V., Buccino, G., Mazziotta, J.C., and Rizzolatti, G. (2005). Grasping the intentions of others with one's own mirror neuron system. PLoS Biol. 3, e79.

10. Hamilton, A.F., and Grafton, S.T. (2008). Action outcomes are represented in human inferior frontoparietal cortex. Cereb. Cortex 18, 1160–1168.

11. Hamilton, A.F., and Grafton, S.T. (2006). Goal representation in human anterior intraparietal sulcus. J. Neurosci. 26, 1133–1137.

12. Giese, M.A., and Rizzolatti, G. (2015). Neural and Computational Mechanisms of Action Processing: Interaction between Visual and Motor Representations. Neuron 88, 167–180.

13. Koul, A., Cavallo, A., Ansuini, C., and Becchio, C. (2016). Doing It Your Way: How Individual Movement Styles Affect Action Prediction. PLoS ONE 11, e0165297.

14. Ting, L.H., Chiel, H.J., Trumbower, R.D., Allen, J.L., McKay, J.L., Hackney, M.E., and Kesar, T.M. (2015). Neuromechanical principles underlying movement modularity and their implications for rehabilitation. Neuron 86, 38–54.

15. Bernstein, N. (1967). The co-ordination and regulation of movements (Pergamon Press Ltd).

16. Stokes, M., and Spaak, E. (2016). The Importance of Single-Trial Analyses in Cognitive Neuroscience. Trends Cogn. Sci. 20, 483–486.

17. Panzeri, S., Harvey, C.D., Piasini, E., Latham, P.E., and Fellin, T. (2017). Cracking the Neural Code for Sensory Perception by Combining Statistics, Intervention, and Behavior. Neuron 93, 491–507.

18. Pica, G., Piasini, E., Safaai, H., Runyan, C.A., Diamond, M.E., Fellin, T., Kayser, C., Harvey, C.D., and Panzeri, S. (2017). Quantifying how much sensory information in a neural code is relevant for behavior. Advances in Neural Information Processing Systems 30, 3686–3696.

19. Zuo, Y., Safaai, H., Notaro, G., Mazzoni, A., Panzeri, S., and Diamond, M.E. (2015). Complementary contributions of spike timing and spike rate to perceptual decisions in rat S1 and S2 cortex. Curr. Biol. 25, 357–363.

20. Avenanti, A., Paracampo, R., Annella, L., Tidoni, E., and Aglioti, S.M. (2018). Boosting and Decreasing Action Prediction Abilities Through Excitatory and Inhibitory tDCS of Inferior Frontal Cortex. Cereb. Cortex 28, 1282–1296.

21. de Wit, M.M., and Buxbaum, L.J. (2017). Critical Motor Involvement in Prediction of Human and Non-biological Motion Trajectories. J. Int. Neuropsychol. Soc. 23, 171–184.

22. Jacquet, P.O., and Avenanti, A. (2015). Perturbing the action observation network during perception and categorization of actions' goals and grips: state-dependency and virtual lesion TMS effects. Cereb. Cortex 25, 598–608.

23. Jastorff, J., Begliomini, C., Fabbri-Destro, M., Rizzolatti, G., and Orban, G.A. (2010). Coding observed motor acts: different organizational principles in the parietal and premotor cortex of humans. J. Neurophysiol. 104, 128–140.

24. Pazzaglia, M., Smania, N., Corato, E., and Aglioti, S.M. (2008). Neural underpinnings of gesture discrimination in patients with limb apraxia. J. Neurosci. 28, 3030–3041.

25. Oosterhof, N.N., Wiggett, A.J., Diedrichsen, J., Tipper, S.P., and Downing, P.E. (2010). Surface-based information mapping reveals crossmodal vision-action representations in human parietal and occipitotemporal cortex. J. Neurophysiol. 104, 1077–1089.

26. Valchev, N., Tidoni, E., Hamilton, A.F.C., Gazzola, V., and Avenanti, A. (2017). Primary somatosensory cortex necessary for the perception of weight from other people's action: A continuous theta-burst TMS experiment. Neuroimage *152*, 195–206.

27. Tidoni, E., Borgomaneri, S., di Pellegrino, G., and Avenanti, A. (2013). Action simulation plays a critical role in deceptive action recognition. J. Neurosci. *33*, 611–623.

28. Urgesi, C., Candidi, M., and Avenanti, A. (2014). Neuroanatomical substrates of action perception and understanding: an anatomic likelihood estimation meta-analysis of lesion-symptom mapping studies in brain injured patients. Front. Hum. Neurosci. *8*, 344.

29. Koul, A., Cavallo, A., Cauda, F., Costa, T., Diano, M., Pontil, M., and Becchio, C. (2018). Action Observation Areas Represent Intentions From Subtle Kinematic Features. Cereb. Cortex *28*, 2647–2654.

30. Pearl, J. (2011). Causality: Models, reasoning, and inference, Second Edition (Cambridge, UK: Cambridge University Press).

31. Jazayeri, M., and Afraz, A. (2017). Navigating the Neural Space in Search of the Neural Code. Neuron *93*, 1003–1014.

32. Panzeri, S., Brunel, N., Logothetis, N.K., and Kayser, C. (2010). Sensory neural codes using multiplexed temporal scales. Trends Neurosci. *33*, 111–120.

33. deCharms, R.C., and Zador, A. (2000). Neural representation and the cortical code. Annu. Rev. Neurosci. *23*, 613–647.

34. Michael, J., Sandberg, K., Skewes, J., Wolf, T., Blicher, J., Overgaard, M., and Frith, C.D. (2014). Continuous theta-burst stimulation demonstrates a causal role of premotor homunculus in action understanding. Psychol. Sci. *25*, 963–972.

35. Valchev, N., Gazzola, V., Avenanti, A., and Keysers, C. (2016). Primary somatosensory contribution to action observation brain activity-combining fMRI and cTBS. Soc. Cogn. Affect. Neurosci. *11*, 1205–1217.

36. Breslow, N.E., and Clayton, D.G. (1993). Approximate Inference in Generalized Linear Mixed Models. J. Am. Stat. Assoc. *88*, 9–25.

37. Becchio, C., and Panzeri, S. (2019). Sensorimotor communication at the intersection between kinematic coding and readout: Comment on "The body talks: Sensorimotor communication and its brain and kinematic signatures" by Giovanni Pezzulo, Francesco Donnarumma, Haris Dindo, Alessandro D'Ausilio, Ivana Konvalinka, Cristiano Castelfranchi. Phys. Life Rev. *28*, 39–42.

38. Hastie, T., Tibshirani, R., and Wainwright, M. (2015). Statistical Learning with Sparsity: the Lasso and Generalizations (Chapman and Hall/CRC).

39. Norton, E.C., and Dowd, B.E. (2018). Log Odds and the Interpretation of Logit Models. Health Serv. Res. *53*, 859–878.

40. Jacob, P., and Jeannerod, M. (2005). The motor theory of social cognition: a critique. Trends Cogn. Sci. *9*, 21–25.

41. Clark, A. (2015). Surfing uncertainty: Prediction, action, and the embodied mind (Oxford University Press).

42. Cattaneo, L., Sandrini, M., and Schwarzbach, J. (2010). State-dependent TMS reveals a hierarchical representation of observed acts in the temporal, parietal, and premotor cortices. Cereb. Cortex *20*, 2252–2258.

43. Pobric, G., and Hamilton, A.F. (2006). Action understanding requires the left inferior frontal cortex. Curr. Biol. *16*, 524–529.

44. Makris, S., and Urgesi, C. (2015). Neural underpinnings of superior action prediction abilities in soccer players. Soc. Cogn. Affect. Neurosci. *10*, 342–351.

45. Thurman, S.M., Giese, M.A., and Grossman, E.D. (2010). Perceptual and computational analysis of critical features for biological motion. J. Vis. *10*, 15.

46. Wadge, H., Brewer, R., Bird, G., Toni, I., and Stolk, A. (2019). Communicative misalignment in Autism Spectrum Disorder. Cortex *115*, 15–26.

47. Cook, J. (2016). From movement kinematics to social cognition: the case of autism. Philos. Trans. R. Soc. Lond. B Biol. Sci. *371*, 20150372.

48. Tzourio-Mazoyer, N., Landeau, B., Papathanassiou, D., Crivello, F., Etard, O., Delcroix, N., Mazoyer, B., and Joliot, M. (2002). Automated anatomical labeling of activations in SPM using a macroscopic anatomical parcellation of the MNI MRI single-subject brain. Neuroimage *15*, 273–289.

49. Mishory, A., Molnar, C., Koola, J., Li, X., Kozel, F.A., Myrick, H., Stroud, Z., Nahas, Z., and George, M.S. (2004). The maximum-likelihood strategy for determining transcranial magnetic stimulation motor threshold, using parameter estimation by sequential testing is faster than conventional methods with similar precision. J. ECT *20*, 160–165.

50. Brett, M., Anton, J., Valabregue, R., and Poline, J. (2002). Region of interest analysis using an SPM toolbox. Neuroimage *16*.

51. Hanke, M., Halchenko, Y.O., Sederberg, P.B., Hanson, S.J., Haxby, J.V., and Pollmann, S. (2009). PyMVPA: A python toolbox for multivariate pattern analysis of fMRI data. Neuroinformatics *7*, 37–53.

52. Friedman, J., Hastie, T., and Tibshirani, R. (2010). Regularization Paths for Generalized Linear Models via Coordinate Descent. J. Stat. Softw. *33*, 1–22.

53. Bates, D., Machler, M., Bolker, B.M., and Walker, S.C. (2015). Fitting Linear Mixed-Effects Models Using lme4. J. Stat. Softw. *67*.

54. Hothorn, T., Bretz, F., and Westfall, P. (2008). Simultaneous Inference in General Parametric Models. Biom. J. *50*, 346–363.

55. Cavallo, A., Koul, A., Ansuini, C., Capozzi, F., and Becchio, C. (2016). Decoding intentions from movement kinematics. Sci. Rep. *6*, 37036.

56. Oldfield, R.C. (1971). The assessment and analysis of handedness: the Edinburgh inventory. Neuropsychologia *9*, 97–113.

57. Rossini, P.M., Burke, D., Chen, R., Cohen, L.G., Daskalakis, Z., Di Iorio, R., Di Lazzaro, V., Ferreri, F., Fitzgerald, P.B., George, M.S., et al. (2015). Non-invasive electrical and magnetic stimulation of the brain, spinal cord, roots and peripheral nerves: Basic principles and procedures for routine clinical and research application. An updated report from an I.F.C.N. Committee. Clin. Neurophysiol. *126*, 1071–1107.

58. Rossi, S., Hallett, M., Rossini, P.M., and Pascual-Leone, A.; Safety of TMS Consensus Group (2009). Safety, ethical considerations, and application guidelines for the use of transcranial magnetic stimulation in clinical practice and research. Clin. Neurophysiol. *120*, 2008–2039.

59. World Medical Association (2013). World Medical Association Declaration of Helsinki: ethical principles for medical research involving human subjects. JAMA *310*, 2191–2194.

60. Yarkoni, T., Poldrack, R.A., Nichols, T.E., Van Essen, D.C., and Wager, T.D. (2011). Large-scale automated synthesis of human functional neuroimaging data. Nat. Methods *8*, 665–670.

61. Huang, Y.Z., Edwards, M.J., Rounis, E., Bhatia, K.P., and Rothwell, J.C. (2005). Theta burst stimulation of the human motor cortex. Neuron *45*, 201–206.

62. Bertini, C., Leo, F., Avenanti, A., and Làdavas, E. (2010). Independent mechanisms for ventriloquism and multisensory integration as revealed by theta-burst stimulation. Eur. J. Neurosci. *31*, 1791–1799.

63. Franca, M., Koch, G., Mochizuki, H., Huang, Y.Z., and Rothwell, J.C. (2006). Effects of theta burst stimulation protocols on phosphene threshold. Clin. Neurophysiol. *117*, 1808–1813.

64. Huang, Y.Z., Rothwell, J.C., Chen, R.S., Lu, C.S., and Chuang, W.L. (2011). The theoretical model of theta burst form of repetitive transcranial magnetic stimulation. Clin. Neurophysiol. *122*, 1011–1018.

65. Wischnewski, M., and Schutter, D.J. (2015). Efficacy and Time Course of Theta Burst Stimulation in Healthy Humans. Brain Stimul. *8*, 685–692.

66. Ghio, M., Vaghi, M.M.S., Perani, D., and Tettamanti, M. (2016). Decoding the neural representation of fine-grained conceptual categories. Neuroimage *132*, 93–103.

67. Ruschel, M., Knösche, T.R., Friederici, A.D., Turner, R., Geyer, S., and Anwander, A. (2014). Connectivity architecture and subdivision of the human inferior parietal cortex revealed by diffusion MRI. Cereb. Cortex *24*, 2436–2448.

68. Yeshurun, Y., Carrasco, M., and Maloney, L.T. (2008). Bias and sensitivity in two-interval forced choice procedures: Tests of the difference model. Vision Res. *48*, 1837–1851.

69. Djurdjevic, V., Ansuini, A., Bertolini, D., Macke, J.H., and Zoccolan, D. (2018). Accuracy of Rats in Discriminating Visual Objects Is Explained by the Complexity of Their Perceptual Strategy. Curr. Biol. *28*, 1005–1015.e5.

70. Parra, L.C., Spence, C.D., Gerson, A.D., and Sajda, P. (2005). Recipes for the linear analysis of EEG. Neuroimage *28*, 326–341.

71. Zou, H., and Hastie, T. (2005). Regularization and variable selection via the elastic net. J. R. Stat. Soc. B Stat. Methodol. *67*, 301–320.

72. Schwarz, G. (1978). Estimating the dimension of a model. Ann. Stat. *6*, 461–464.

73. Agresti, A. (2007). An Introduction to the Categorical Data Analysis (John Wiley & Sons, Inc.).

74. Luke, S.G. (2017). Evaluating significance in linear mixed-effects models in R. Behav. Res. Methods *49*, 1494–1502.

75. Brysbaert, M., and Stevens, M. (2018). Power analysis and effect size in mixed effects models: A tutorial. J. Cogn. *1*, 9.

76. Best, D., and Roberts, D. (1975). Algorithm AS 89: the upper tail probabilities of Spearman's rho. J. R. Stat. Soc. C Appl. Stat. *24*, 377–379.

77. Kendall, M.G. (1975). Rank Correlatin Methods (Charles Griffin).

STAR★METHODS

KEY RESOURCES TABLE

REAGENT or RESOURCE	SOURCE	IDENTIFIER
Deposited Data		
Data supporting main findings	This paper	Mendeley Data: https://doi.org/10.17632/6jzbrkjpty.1
Software and Algorithms		
Adobe Premiere Pro	Adobe	https://www.adobe.com/products/premiere.html
AAL	[48]	http://www.gin.cnrs.fr/spip.php?article216; RRID:SCR_003550
Motor Threshold Assessment Tool 2.0	[49]	https://www.clinicalresearcher.org/software.htm
MarsBaR region of interest toolbox for SPM	[50]	http://marsbar.sourceforge.net/; RRID:SCR_009605
SofTaxic software	EMS srl	http://www.softaxic.com/
E-prime	Psychology Software Tools, Pittsburgh, PA	https://pstnet.com/; RRID:SCR_009567
PyMVPA	[51]	http://www.pymvpa.org/
glmnet	[52]	https://cran.r-project.org/web/packages/glmnet/index.html; RRID:SCR_015505
R package: lme4	[53]	https://cran.r-project.org/web/packages/lme4/index.html; RRID:SCR_015654
R package: multcomp	[54]	https://cran.r-project.org/web/packages/multcomp/index.html; RRID:SCR_018255
MATLAB	MathWorks Inc.	http://www.mathworks.com/products/matlab/; RRID:SCR_001622

RESOURCE AVAILABILITY

Lead Contact
Further information and requests for resources should be directed and will be fulfilled by the Lead contact, Stefano Panzeri (stefano.panzeri@iit.it).

Materials Availability
This study did not generate new unique reagents or materials.

Data and Code Availability
The data supporting the main findings of this study are available for download at the following link (https://doi.org/10.17632/6jzbrkjpty.1). The code supporting the main findings of this study is based on public available tools listed in the Key Resource Table. Custom functions inputting data to toolboxes will be made available by the Lead contact upon reasonable request.

EXPERIMENTAL MODEL AND SUBJECT DETAILS

Based on [55], we decided *a priori* to collect data from at least 15 participants in each task. We calculated a minimum sample size *a priori* on the basis of the effect size of 1.091 reported by [55] (action observation, study 1; comparison against chance; given H0 = 0.5; Mean ± SD. H1 = 0.608 ± 0.099). This analysis indicated that we would need a minimum of 15 participants to achieve 99% power to detect a similar effect (effect size = 1.091; $\alpha = 0.05$; power $(1-\beta) = 0.99$). Considering the efficacy of cTBS, we increased this estimate and tested 20 participants in each task. Three participants were removed from the sample as they did not complete all the three sessions. Additionally, two participants were unable to complete the cTBS sessions due to a too-high resting motor threshold (above 80% of maximal stimulator output). Thus, n = 16 for the intention discrimination task (10 females, 6 males, mean age 23, range 19-27 years) and n = 19 for the kinematic discrimination task (9 females, 10 males, mean age 24, range 20-28 years). All participants were right-handed according to the Edinburgh Handedness Inventory [56] and had normal or corrected to normal vision. None of the participants reported neurological, psychiatric, or other medical problems or any contraindication to MRI or TMS [57, 58]. Informed written consent was obtained in accordance with the principles of the revised Helsinki Declaration [59] and with procedures cleared by the local ethics committee (Comitato di Bioetica di Ateneo, University of Turin). All participants received monetary compensation for their time.

METHOD DETAILS

Experimental design and procedures

The design of the intention discrimination and kinematic discrimination tasks was between-subjects, while effects of cTBS used a within-subject design. Participants assigned to each task underwent a high-resolution MRI structural scan, after which they attended three experimental sessions: no cTBS, cTBS to the left IPL and cTBS to the left IFG. During each of these sessions, participants completed the intention discrimination task (or the kinematic discrimination task, depending on task assignment) followed by a contrast discrimination task to control for cTBS effects unrelated to action observation. Participants sat in front of a 24-in. inch computer screen (resolution 1280 × 800 pixels, refresh frequency 60 Hz) at a distance of 50 cm in a dimly lit room. Each session lasted approximately 90 minutes and occurred at the same time of the day (±1 h) for each participant. Participant sessions were separated by one week, and session type order was randomized across participants.

MRI acquisition

T1-weighted scans were acquired using a 1.5 Tesla INTERA scanner (Philips Medical Systems) equipped with a 32-channel SENSE high-field head coil. Each high-resolution structural scan included 160 axial slices with an in-plane field of view (FOV) of 256 × 240 and a gap of 0 mm for a resolution of 1 × 1 x 1 mm (TR = 8.2 ms, TE = 3.80 ms, flip angle = 8 degrees). T1-weighted scans were used for the MRI-guided neuronavigation used to target cTBS stimulation sites (see below).

MRI-guided cTBS protocol

MRI-guided cTBS was administered using a 70-mm figure-eight coil connected to a Magstim Rapid2 stimulator (Magstim, Dyfed, UK). A SofTaxic NeuroNavigator system (EMS, Bologna, Italy) was employed to determine the coil position for all the 'to-be-stimulated' brain regions. Specifically, individual MRI scans were used to first construct scalp surface and skull landmarks of the left peri-auricular (A1), right periauricular (A2) and nasion (N) on the participant's T1 MRI image. The brain scan was then normalized to Talairach space and neuronavigation data were co-registered to measurements taken from the same points of reference (A1, A2, N) sampled from the participant's scalp. The intensity for the cTBS protocol was set at 90% of the resting Motor Threshold (rMT), defined as minimal stimulation intensity producing motor evoked potentials (MEPs) of a minimum amplitude of 50 μV in the first dorsal interosseous (FDI) muscle [57]. To determine the rMT, for each participant for each stimulation session, we applied single pulse TMS over the left Primary Motor Cortex (M1) and recorded the MEPs from the right FDI muscle using a Biopac MP-150 (Biopac Systems, Inc., Santa Barbara, CA) through pairs of Ag–AgCl surface electrodes in a belly tendon montage. The rMT was determined by means of adaptive parameter estimation by sequential testing procedure (PEST) with the Motor Threshold Assessment Tool 2.0 [49]. The coordinates for targeting left M1 (Talairach x = −44, y = −19, z = 53) were extracted from the neurosynth reverse inference map for the term 'index finger' [60]. Following the rMT estimation procedure, cTBS was delivered to the left IFG and the left IPL targets. cTBS consisted of three pulses at 50 Hz repeatedly applied at intervals of 200 ms (5 Hz) for 40 s [61]. In cTBS sessions, discrimination tasks were administered 5 min post cTBS, that is, in the time window in which maximal inhibitory effects of stimulation have been reported [61–65].

cTBS targets

cTBS targets were defined based on a new analysis of beta images obtained from 20 volunteers watching the same action stimuli used in this study while undergoing fMRI [29]. Each volunteer completed three fMRI runs resulting in a total of 120 beta images (20 participants x 3 runs x 2 intentions). MVPA analysis was performed with PyMVPA [51]. For each participant, the time course of the blood oxygen level-dependent (BOLD) signal for each voxel was z-scored for each run and then averaged across runs for each intention to decrease intra-subject variability and improve the signal to noise ratio [66]. We defined separate anatomical regions of interest (ROIs) using the Automated Anatomical Labeling (AAL) [48] library contained in MarsBaR SPM toolbox [50]. We trained and tested separate linear SVM classifier to distinguish between intentions within each ROI with accuracy assessed using leave-one-sub-ject-out (LOSO) cross validation (see Table S1 for classification accuracies in all ROIs). For IFG, we extracted separate ROIs for IFG *pars opercularis*, *pars triangularis*, and *pars orbitalis*. Intentions were classified most accurately in the left IFG *pars orbitalis*. The MVPA-defined cTBS target (MNI x = −46, y = 30, z = −12, then converted to Talairach stereotactic coordinates x = −46, y = 29, z = −12) was chosen in a central portion of the left IFG *pars orbitalis* that contained a large number of informative voxels (20% highest ranked voxels; see Figure S1A). For IPL, intentions were classified with an accuracy of 0.78 in the left IPL. The MVPA-defined cTBS target (MNI coordinates x = −58, y = −34, z = 40, then converted to Talairach stereotactic coordinates x = −57, y = −31, z = 38) was chosen in the anterior part of the left IPL [67], which again contained a large number of voxels ranked as most informative (20% highest ranked voxels; Figure S1A). The SofTaxic neuronavigational system (E.M.S. srl, Bologna, Italy) located the corresponding scalp position with an error threshold set to the default value of 2 mm.

Acquisition and analysis of kinematic data

Stimuli were selected from a dataset of 512 grasping acts obtained by recording 17 naive participants reaching toward and grasping a bottle to pour some water into a small glass or drink water from the bottle. Detailed apparatus and procedures are described in [55]. Briefly, reach-to-grasp movements were tracked using a near-infrared camera motion capture system with nine cameras (frame rate, 100 Hz; Vicon System) and concurrently filmed from a lateral viewpoint using a digital video camera (Sony Handy Cam 3-D, 25 frames/sec). Computation of kinematic variables was based on [55] and followed identical procedures. We used a custom software (MATLAB; MathWorks Inc., Natick, MA) to compute two sets of kinematic variables of interest: F_{global} variables and F_{local} variables. F_{global} variables (n = 4) were expressed with respect to the global frame of reference, i.e., the frame of reference of the motion capture system. Within this frame of reference, we computed the following variables (also listed in Table 1):

Table 1. Kinematic Variables of Interest

Kinematic Variables	Definition
Wrist velocity (W_V)	module of the velocity of the wrist marker (millimeters per second)
Wrist height (W_H)	z (i.e., up-down) component of the wrist marker (millimeters)
Wrist horizontal trajectory (W_{HT})	x (i.e., left-right) component of the wrist marker (millimeters)
Grip aperture (GA)	distance between the marker placed on the tip of the thumb and the marker placed on the tip of the index finger (millimeters)
x, y, z index (I_X, I_Y, I_Z)	x, y, and z coordinates for the index (millimeters)
x, y, z thumb (T_X, T_Y, T_Z)	x, y, and z coordinates for the thumb (millimeters)
x, y, z finger plane (FP_X, FP_Y, FP_Z)	x, y, and z components of the thumb-index plane (millimeters)
x, y, z dorsum plane (DP_X, DP_Y, DP_Z)	x, y, and z components of the radius-phalanx plane (millimeters)

Kinematic variables were computed throughout the reach-to-grasp phase of grasp-to-pour and grasp-to-drink acts from reach onset to reach offset.

- wrist velocity, defined as the module of the velocity of the wrist marker (mm/sec);
- wrist height, defined as the z-component of the wrist marker (mm);
- wrist horizontal trajectory, defined as the x-component of the wrist marker (mm);
- grip aperture, defined as the distance between the marker placed on thumb tip and the one placed on the tip of the index finger (mm).

To provide a better characterization of the hand joint movements, the second set of variables was expressed with respect to a local frame of reference centered on the hand (i.e., F_{local}). Within F_{local} we computed the following variables:

- x-, y-, and z-thumb defined as x-, y- and z-coordinates for the thumb with respect to F_{local} (mm);
- x-, y-, and z-index defined as x-, y- and z-coordinates for the index with respect to F_{local} (mm);
- x-, y-, and z-finger plane defined as x-, y- and z-components of the thumb-index plane, i.e., the three-dimensional components of the vector that is orthogonal to the plane, providing information about the abduction/adduction movement of the thumb and index finger irrespective of the effects of wrist rotation and of finger flexion/extension;
- x-, y-, and z-dorsum plane defined as x-, y- and z-components of the radius-phalanx plane, providing information about the abduction, adduction and rotation of the hand dorsum irrespective of the effects of wrist rotation.

Selection of action stimuli

From the full dataset of 512 grasping acts, we selected 60 grasping acts (30 grasp-to-pour; 30 grasp-to-drink) to satisfy the following requirements: i) within-intention distance was minimized (using the metric reported in [55]); ii) median split based on maximum wrist height led to a significant difference between "higher" and "lower" wrist height grasps (t_{58} = 11.2; p < 0.001); iii) peak wrist height did not differ between intentions (p = 0.27). These requirements ensured that both intention and peak wrist information were available and that correct response in the kinematic discrimination task was not systematically associated with a given intention (e.g., higher peak wrist height associated with grasp-to-drink). Movies corresponding to the selected reach-to-grasp acts were used as stimuli in the intention discrimination task and in the kinematic discrimination task. Movies were edited with Adobe Premiere Pro CS6 (mp4 format, disabled audio, 25 frames per second, resolution 1,280 × 800 pixels) so that each movie clip started with the reach onset and ended at contact time between the hand and the bottle. Movement duration (mean ± SEM = 1.04 ± 0.02 s, range = 0.84 to 1.36 s) did not differ between intentions (t_{58} = −0.30; p = 0.76). To allow participants enough time to focus on movement start, 9, 11, or 13 static frames were randomly added at the beginning of each video. In order to equate video durations, static frames were also added at the end of each videos in a compensatory manner.

Intention discrimination task

The intention discrimination task consisted of two blocks of 60 trials. Task structure conformed to a 2AFC design. Each trial displayed two reach-to-grasp acts in two consecutive temporal intervals: one interval contained a grasp-to-pour act, the other a grasp-to-drink act. Depending on block, participants had to indicate the interval (first or second) containing the grasp-to-drink or grasp-to-pour act. Each trial started with the presentation of a white central fixation cross for 1500 ms. Then, the first grasping act was presented followed by an inter-stimulus interval of 500 ms, after which the second grasping act was presented. After the end of the second video, the screen prompted participants to indicate the interval (first or second) containing the grasp-to-drink (or grasp-to-pour, depending on block) action by pressing a key. The prompt screen was displayed until response or for a maximum duration of 3000 ms. After response, participants were requested to rate the confidence of their choice on a four-level scale by pressing a key. Pairing of videos was randomized across trials and participants. Participants began the session by performing a practice block before the main experimental task. The order of the presentation of the blocks was counterbalanced across participants. Participants received no feedback, neither during the experimental blocks nor during the practice block. Control analyses revealed no difference in performance across trials within a block, and also no difference in performance between the two blocks (Tables S3 and S5). Stimulus presentation, timing and randomization was controlled using E-prime V2.0 software (Psychology Software Tools, Pittsburgh, PA).

Kinematic discrimination task

The kinematic discrimination task included the same stimuli and design as the intention discrimination task, except that participants were asked to indicate the interval containing the grasp with higher (or lower, depending on block) peak vertical height of the wrist.

Control for decision biases

To identify response biases, we assessed the probability of answering "to drink" in the intention task and "higher" in the kinematic task against chance and across sessions and found no difference. Additionally, to rule out that the decrease in intention discrimination following IPL cTBS was due to an asymmetry in performance in the two intervals (interval bias [68]), we conducted an additional control analysis to compare the probability of correct response in the first versus the second interval across sessions. If the decrease in intention discrimination under IPL cTBS reflected an interval bias, we would expect an interaction between interval and session. This was not the case. While the probability of correct response when the signal was in the first interval was overall higher than the probability of correct response when the signal was in the second interval, the interaction between interval and session was not significant (Table S3). The pattern of results was similar for the kinematic discrimination task (Table S3).

Control contrast discrimination task

To control for cTBS effects unrelated to action observation, such as integration of evidence favoring one alternative over time, participants performed a contrast discrimination task at the end of each session. The contrast discrimination task consisted of three blocks of 32 trials. Each trial started with the presentation of a fixation cross (1000 ms), after which two gray rectangles were displayed for 1000 ms on two consecutive intervals separated by a 500 ms inter-stimulus interval. We adjusted the Michelson contrast of the images so that, in half of the trials, the rectangles did not differ in contrast (Michelson contrast = 0%), and, in the other half of the trials, the rectangles had a Michelson contrast of 4.76%, 6.98%, 9.09% or 11.11%. For each trial, the participant had to indicate whether the contrast of the rectangles was 'same' or 'different' (within a 3000 ms window) and rate the confidence of their choice on a four-level scale by pressing a key. Trials for which subjects failed to provide a response within 3000 ms were discarded from the analyses (0.5% of trials performed by subjects in the intention discrimination group and 0.3% of trials performed by subjects in the kinematic discrimination group). Task performance revealed no influence of IPL cTBS or IFG cTBS across sessions and tasks (p > 0.05 in all cases) (Table S3).

QUANTIFICATION AND STATISTICAL ANALYSIS

Data preprocessing

Trials for which subjects failed to provide a response within 3000 ms were discarded from the analyses (0.5% of trials for the intention discrimination task and 0.1% of trials for the kinematic discrimination task). The first 25% of trials in each block were discarded to account for the time needed by participants to familiarize with task and response mapping. As a control, we verified that the pattern of results and their significance remained similar even when including all trials. Specifically, similarly to Figure 1D, we found a significant decrease in intention discrimination post IPL cTBS relative to both no cTBS and IFG cTBS. Kinematic discrimination did not differ across sessions.

Single-trial kinematic vector

To model single-trial kinematics, we first averaged, for each grasping act, the 16 kinematic variables of interest over four epochs of 25% of the normalized movement time (0%–25%, 25%–50%, 50%–75%, and 75%–100% of movement duration defined from reach onset to reach offset). Next, for each trial, we combined the kinematic features associated with the two grasping acts in a 64-dimensional kinematic vector, $\vec{K}$, defined as:

$$\vec{K} = \vec{K_1} - \vec{K_2}$$

(Equation 1)

where $\vec{K_1}$ and $\vec{K_2}$ denote the vectors of kinematic features associated to the first and second reach-to-grasp act displayed in the trials. This definition, used in all of our logistic regression analyses, reflects the assumption that, in a 2AFC task, choices are based on comparative judgements. Using more detailed regression models that employed the kinematic features of the two grasping acts did not improve model predictability (Figure S3). Given that the model using the full set of kinematic features had twice as many predictors as the model using the difference (128 versus 64 dimensions), but only led to a null to marginal increase in model performance, for the sake of parsimony, we used the simpler model in all analyses.

We also explored whether the number of time epochs used for the discretization of the temporal evolution of kinematic variables influenced model performance. We compared the performance of the four-time-epoch readout model, used in all the analyses presented in the main text and supplemental figures, with that of models based on finer time discretization (six or eight time epochs). Six- and eight-time epoch models performed no better than the four-time epoch model (p > 0.4 for all sessions, tasks and number of epochs).

Logistic regression models of encoding and readout

We analyzed encoding and readout using two sets of logistic regression models: encoding and readout models. Logistic regression is a linear regression for log-odds [38], and is a standard probabilistic approach to classification. Logistic regression models are powerful for explaining behavioral strategies [69]. They confer several advantages in modeling the dependence of a random binary variable,

such as observers' choice, on one or more explanatory variables [70]. For example, they assume binomial noise – the most natural noise model for binary responses; they combine predictor variables linearly; they can be robustly fit to data; they have a graded nonlinearity, which allows for a modulation of probabilities different from an all-or-none binarization. The latter property is particularly suitable for a readout model as in our data discrimination performance correlated with confidence ratings in the no cTBS session (Spearman's correlation: rho = 0.075, p = 0.005 and rho = 0.308, p < 0.001 for the intention and kinematic discrimination tasks, respectively), suggesting the possibility of a graded dependence of the response probability on the strength of kinematic evidence. To aid comparison between encoding and readout models, we also used logistic regression for modeling encoding. Versions of the encoding models based on other formulations, such as linear discriminant analysis, were also built and tested, and yielded qualitatively similar results.

The logistic model expressed the probability of a binary stochastic variable Y, where Y takes the values 'to drink' and 'to pour' for intention discrimination, as a sigmoid transformation of the sum of the components of the single-trial kinematic vector $\overrightarrow{K}$. The equation of the model was as follows:

$$P\left(\left[Y = {}'to\ drink'\right]\middle|\overrightarrow{K}\right) = \sigma\left(\overrightarrow{K} * \overrightarrow{\beta} + \beta_0\right)$$

$$P\left(\left[Y = {}'to\ pour'\right]\middle|\overrightarrow{K}\right) = 1 - P\left(\left[Y = {}'to\ drink'\right]\middle|\overrightarrow{K}\right) \qquad \text{(Equation 2)}$$

where σ is the sigmoid function, $\overrightarrow{\beta}$ is the vector containing the values of the regression coefficients of each kinematic feature, and β_0 is the bias, kinematic independent, term.

Training logistic regression models

Training and evaluation were performed similarly for both sets of models and for both discrimination tasks. Each model was trained on the set of the 90 trials retained for analyses. We z-scored the single-trial kinematic vectors within each model in order to avoid penalizing predictors with larger ranges of values. To avoid over-fitting, we trained each model using elastic-net regularization, with a value of $\alpha = 0.95$ for the elastic net parameter, which provides sparser solutions in parameter space [71]. To check whether the pattern of readout weights was robust to the choice of the elastic net hyper-parameter α, we computed for each participant the correlation between the readout weights for $\alpha = 0.95$ with the readout weights obtained with values of α ranging from 0.5 to 1. Correlation values decreased with α values but remained higher than 0.9 for all $\alpha > 0.5$. Thus, readout results were robust to the choice of α. The parameter λ, which controls the strength of the regularization term, was estimated for each model using leave-one-out cross-validation. We retained for each model the value λ_{min} associated to the minimum mean cross-validated error. Models were trained on all 90 trials with the retained regularization term. Logistic regression was implemented using *R glmnet* package [52].

In the main text, we report the results obtained by applying this training procedure as it gives only one set of regression coefficients per analyzed case and it is therefore easier to interpret. However, qualitatively similar results were obtained when using leave-one out cross validation on the entire procedure (on top of the cross validation used for the determination of the λ parameter). The fully cross-validated performance of encoding models remained close to 100% for both the intention and the kinematic discrimination tasks (99.5 ± 0.1% and 98.1 ± 0.2% for the intention discrimination task and kinematic discrimination task, respectively). The fully cross-validated performance of readout models also remained significantly above chance in all sessions and tasks (p < 0.001, adjusted for the three comparisons in each task). The correlation between observed and predicted task performance also remained significant in all cases (p < 0.001). Moreover, alignment was still significantly decreased after IPL cTBS as compared to no cTBS (p < 0.01).

Verification of the statistical significance of non-zero regression coefficients

To check that the regularization was working well and that the regression coefficients with non-zero value were meaningful [38], we did a permutation test in which a null hypothesis distribution of regression weights was obtained after random permutations of the trial labels. We took the absolute value of each individual regression coefficient obtained in the permuted dataset to build a distribution of absolute values of regression coefficient expected under the null-hypothesis of no relationship between the kinematics and the variable Y. We verified that all non-zero beta coefficients had an absolute value that exceeded the 95th percentile of this null-hypothesis distribution.

Encoding model

The intention encoding model expressed the probability of the grasping act displayed in the first interval of a given trial being 'to drink' as a function of the kinematic vector measured in the same trial. Having verified that intention information slightly varied as a function of video pairings (which were randomized across trials and participants), we trained the encoding model separately on each set of video pairings presented in each session to each observer. We used the encoding model to evaluate the overall amount of intention information in movement kinematics (Figures 2F and S2A). The procedures for the kinematic discrimination task were identical.

Readout model

The intention readout model expressed the probability of intention choice in a given trial as a function of the kinematic vector measured in the same trial. We trained the readout model separately for each observer in each session. To model intention choice as a function of single-trial kinematics, we trained the readout model using all 64 kinematic features (16 kinematic variables at four time epochs). The procedures for the kinematic discrimination task were identical.

Evaluation of model performance

To quantify model performance (Figures 2F, 3D, and 3G), we computed for each trial the most likely value of the variable Y by taking the argmax over Y of $P(Y|\vec{K})$ in Equation 2. This parameter provides an estimate of the model prediction (prediction of the actual intention of the instructed action sequence for the encoding model; prediction of observer's intention choice for the readout model) on a single trial. We then quantified model performance as the fraction of correct predictions computed over all the trials. The chance-level null-hypothesis distribution for readout model performance was created by fitting the model after randomly permuting across trials the observer's choice labels.

Computation of task performance predicted by the readout model

In Figures 3E and 3H, we used the readout model to estimate individual discrimination performance, as follows. Using the logistic readout model (Equation 2), we computed for each trial the probability of each choice. Then we averaged across all trials the probability of the correct choice.

Classification of individual kinematic features as informative

To evaluate the informativeness of individual features about intention (which is used for Figures 5, S2A, S2B, and S5), we used a single-feature encoding model implemented using MATLAB's *glmfit* function. Each model was trained on the full set of 90 trials retained for analyses. We z-scored the single-trial kinematic vectors. Significance of the regression coefficient was assessed with t-statistics. We retained as informative kinematic features whose regression coefficients were found to be significant ($p < 0.05$) in all video pairings. In Figures S2A and S2B, variables are ranked in terms of their encoded information. Ranking was determined by computing the average norm of the regression coefficient of each informative feature across all video pairings and then summing the obtained norms across features belonging to the same kinematic variable.

Contribution of individual kinematic variables to discrimination performance

Figures 5D and S5D visualize the contribution of individual kinematic variables to discrimination performance. Single variable contribution to discrimination performance was computed as the scalar product between the kinematic vector and the readout vector calculated within the feature subspace formed by the features of the considered kinematic variable (e.g., 25%, 50%, 75% and 100% of movement time for W_H). Positive (negative) values of this index imply a positive (negative) contribution of the variable toward enhancing (decreasing) discrimination performance.

Computation of cross-correlations of readout coefficients across participants

To quantify the inter-individual reproducibility of the readout regression coefficients, we computed the cross-correlation between the readout coefficients for each different pair of participants separately for each session. We then took the mean ± SEM across all participant pairs, separately for each session. To check that the so obtained low cross-correlation values were robust to the choice of the elastic net hyper-parameter α ($\alpha = 0.95$ was used for all main text analyses), we recomputed the cross-correlations between readout coefficients obtained by performing the regressions using values of α ranging from 0.5 to 1. Cross-correlations slightly increased with lower α values, but remained always below 0.1. These analyses corroborate the idea that the small correlation values in the intention discrimination task reflected genuine inter-individual differences.

Conventions for p values

The *p* values of all reported statistical comparisons are two-sided and Holm-Bonferroni corrected. Tables S3–S5 report the details of Logistic Mixed Effects Models (LMEM), non-parametric permutation tests and correlation analyses, respectively. Details of procedures are reported below. In all figures, * indicates $p < 0.05$, ** indicates $p < 0.01$, *** indicates $p < 0.001$, *ns* indicates $p > 0.05$. Following standard notations, * above bars indicate significance of difference from chance of an individual quantity, * above brackets indicate significance of difference between two quantities.

Logistic Mixed Effects Models for assessing statistical differences in the distribution of binary variables

We used LMEM to assess the significance of differences in discrimination performance (Figures 1D and 1E; Table S3), response bias (Figure S1B), readout model performance (Figures 3D and 3G), and confidence ratings (high versus low; Table S3) against chance and across sessions.

We considered the 0/1 variable in each trial (response for assessing discrimination performance, response predicted by the model for assessing model performance, and response for assessing response bias) as dependent variable, session as categorical predictor and subject identity as random effect. Logistic statistics were used because these quantities are computed from binary stochastic variables in each trial and thus cannot be assessed with t tests or other parametric Gaussian statistics. We selected the random-

effect structure of the model by comparing a random intercept only model (df 4) with a model including both random intercept and random slope (df 9). We performed model selection using the Bayesian Information Criterion (BIC) [72], which rewards model fit and penalizes model complexity (number of df). We carried out model fitting using the R package lme4 [53]. Model selection results are reported in Table S2.

We tested for a main effect of cTBS in discrimination performance by conducting a likelihood-ratio test between Mixed Effects Models differing only in the presence or absence of cTBS conditions as predictor [73]. We conducted comparisons across sessions using the glht command from the R package multcomp [54]. The multcomp package estimated the value and standard error of each effect, from which a z value (for computation of two-sided p values) and a Cohen's d value (for estimation of effect size, by diving the z value by the square root of the number of participants) were computed. We used Cohen's d to quantify effect size in Mixed Effects Model because it is easy to interpret and used throughout the text for many analyses; however, readers should be aware of the debate about which sources of variations should be considered for its computation in Mixed Effect Models [74, 75]. All p values were Holm-Bonferroni corrected for three comparisons (IPL cTBS versus no cTBS, IFG cTBS versus no cTBS, and IPL cTBS versus IFG cTBS).

Permutation test for assessing statistical differences in readout coefficients and alignment

For assessing differences in alignment (Figures 4E and S4D–S4F) and in the contribution of individual features to discrimination performance (Figures 5D and S5D), we used non-parametric permutation statistics based on constructing a null-hypothesis distribution of differences in values after randomly permuting session labels across trials. For assessing significance of differences in the readout regression coefficients computed for each subject across sessions (Figures 5A, 5B, S5A, and S5B), we used a similar session label permutation test for regression coefficients. For all tests, the null-hypothesis distribution was computed using 10^4 random permutations. In all permutation tests, reported p values are two-sided. All p values were Holm-Bonferroni corrected for three comparisons (IPL cTBS versus no cTBS, IFG cTBS versus no cTBS, and IPL cTBS versus IFG cTBS), except for Figures 5 and S5, in which we only compared no cTBS against IPL cTBS.

Statistical significance of correlations

Significance of Pearson's correlation values and stepwise regression coefficients were assessed using two-sided parametric Student statistics [76] implemented in the MATLAB functions *corr* and *stepwisefit,* respectively. We assessed significance of Spearman correlations using the two-sided permutation distribution [77] implemented in the MATLAB function *corr*. All p values were Holm-Bonferroni corrected for three comparisons (IPL cTBS versus no cTBS, IFG cTBS versus no cTBS, and IPL cTBS versus IFG cTBS).